2.2. Garrido-Franco, M., Laber, B., Huber, R. and Clausen, T. (2001). Structural basis for the function of pyridoxine 5'-phosphate synthase. *Structure* **9**:245-253.

Structure with Folding and Design

Structural Basis for the Function of Pyridoxine 5'-Phosphate Synthase

Marta Garrido Franco, Bernd Laber[1], Robert Huber and Tim Clausen[*]

Max-Planck-Institut für Biochemie, Abteilung Strukturforschung, D-82152 Planegg-Martinsried, Germany

[1]Aventis CropScience GmbH, Forschung Biochemie, D-65926 Frankfurt am Main, Germany

[*]Corresponding author, Tel. +49-89-8578 2680, Fax +49-89-8578 3516, email: clausen@biochem.mpg.de

Running Title

Crystal Structure of PNP Synthase

Received: November 14, 2000
Revised: January 9, 2001
Accepted: January 25, 2001

Abbreviations

AAP, 1-amino-acetone-3-phosphate; DXP, 1-deoxy-D-xylulose-5'-phosphate; HTP, 4-phosphohydroxy-L-threonine; IGPS, indoleglycerolphosphate synthase; NCS, non-crystallographic symmetry; P_i, inorganic phosphate; PLP, pyridoxal 5'-phosphate; PMP, pyridoxamine 5'-phosphate; PNP, pyridoxine 5'-phosphate; SIRAS, single isomorphous replacement with anomalous scattering.

Key Words

Enzyme-product complex**;** Open-closed transition; PdxJ; Pyridoxal 5'-phosphate, TIM barrel.

SUMMARY

Background: Pyridoxal 5'-phosphate is the active form of vitamin B_6 that acts as an essential, ubiquitous coenzyme in amino acid metabolism. In *Escherichia coli*, the pathway of the *de novo* biosynthesis of vitamin B_6 results in formation of pyridoxine 5'phosphate (PNP), which can be regarded as the first synthesized B_6 vitamer. PNP synthase (commonly referred to as PdxJ) is a homooctameric enzyme that catalyzes the final step in this pathway, a complex intramolecular condensation reaction between 1-deoxy-D-xylulose-5'-phosphate and 1-amino-acetone-3-phosphate.

Results: The crystal structure of *E. coli* PNP synthase was solved by single isomorphous replacement with anomalous scattering and refined at a resolution of 2.0 Å. The monomer of PNP synthase consists of one compact domain that adopts the abundant TIM barrel fold. Intersubunit contacts are mediated by three additional helices, respective to the classical TIM barrel helices, generating a tetramer of symmetric dimers with 422 symmetry. In the shared active sites of the active dimers, Arg20 is directly involved in substrate binding of the partner monomer. Furthermore, the structure of PNP synthase with its physiological products, PNP and P_i, was determined at 2.3 Å resolution, which provides insight into the dynamic action of the enzyme and allows us to identify amino acids critical for enzymatic function.

Conclusion: The high-resolution structures of the free enzyme and the enzyme-product complex of *E. coli* PNP synthase suggest essentials of the enzymatic mechanism. The main catalytic features are active-site closure upon substrate binding by rearrangement of

one C-terminal loop of the TIM barrel, charge-charge stabilization of the protonated Schiff-base intermediate, the presence of two phosphate-binding sites, and a water channel that penetrates the β barrel and allows the release of water molecules in the closed state. All related PNP synthases are predicted to fold into a similar TIM barrel pattern and have comparable active site architecture. Thus, a common mechanism can be anticipated.

INTRODUCTION

The biocatalytically active form of vitamin B_6, pyridoxal 5'-phosphate (PLP), represents one of nature's most versatile cofactors that plays a central role in amino acid metabolism. PLP-dependent enzymes are involved in various pathways ranging from interconversion of α-amino acids to the synthesis of antibiotic compounds. Like PLP, pyridoxamine 5'-phosphate (PMP) acts as an essential cofactor in the biosynthesis of deoxysugars. Despite its paramount physiological and pharmaceutical importance, little is known about the *de novo* synthesis of vitamin B_6. Biosynthetic studies have been focused on *E. coli*, in which five genes required for synthesis have been identified *via* complementation of auxotrophic mutants and tracing experiments using radioactive labeled precursors (for a review see [1]). While two of the defined genes (*serC* and *gapB*) are also involved in other biosynthetic pathways, the gene products of *pdxA*, *pdxB* and *pdxJ* are unique to B_6 biosynthesis. GapB, SerC and PdxB catalyze the formation of the nonproteinogenic amino acid 4-phosphohydroxy-threonine (HTP), which is one of the two acyclic vitamin B_6 building blocks. PdxA and PdxJ are required for the condensation

of HTP with the second building block, deoxyxylulose 5'-phosphate (DXP), to yield pyridoxine 5'-phosphate (PNP). The different B_6 vitamers, pyridoxine, pyridoxal, pyridoxamine, PLP, and PMP, are generated from PNP and interconverted into each other in the so called salvage pathway by the action of the ATP-dependent kinase PdxK, various transaminases, and the FMN-dependent oxidase PdxH [2-5].

The exact roles of PdxA and PdxJ, however, remained undetermined for a long time. It was demonstrated only recently, that PdxA is an NAD-dependent dehydrogenase that catalyzes the oxidative decarboxylation of HTP to give the unstable intermediate aminoacetone-3-phosphate (AAP) [6]. PdxJ (also referred to as PNP synthase) then catalyzes the consecutive reaction in which AAP and DXP are condensed to yield PNP and inorganic phosphate P_i as indicated in Figure 1 [7-9].

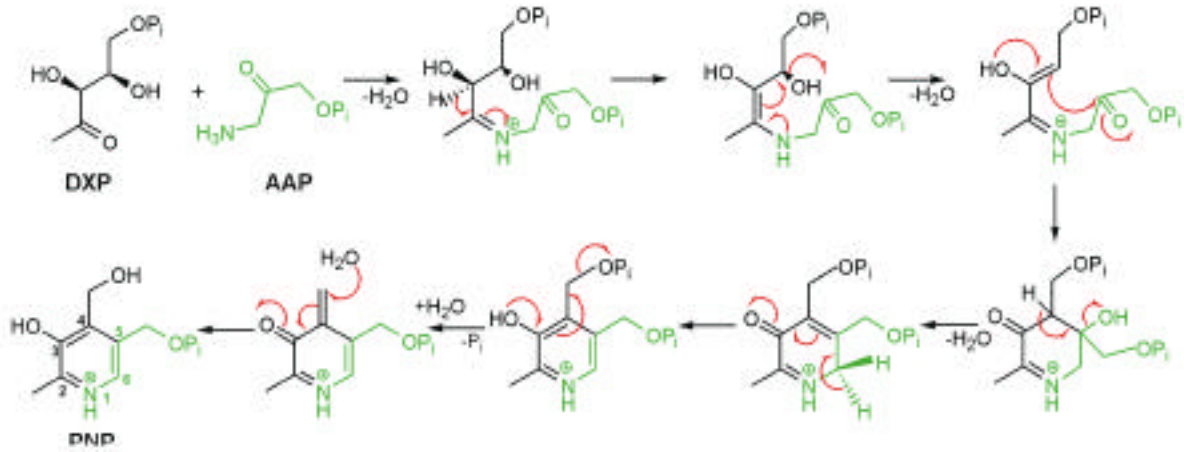

Figure 1. Reaction Catalyzed by PNP Synthase. To illustrate the origin of the PNP skeleton the DXP-derived atoms are colored in black, and the AAP-derived atoms are colored in green. The precise sequence was adapted from Cane and coworkers [9].

Recent findings suggest that vitamin B_6 functions, in addition to its vital coenzyme role, as an antioxidant that quenches singulet molecular oxygen during photooxidative stress [10, 11]. The gene *SOR1* (singulet oxygen resistance, also called *pdx1*, *pyroA*) was

identified in *Cercospora nicotianae* and *Aspergillus nidulans* as the responsible element for this resistance [12, 13]. As it was demonstrated in further experiments, the SOR1 protein is specifically required for pyridoxine biosynthesis, although no homology to any of the well known *E. coli pdx* genes exists. Sequence database analysis indicated that organisms encode either *SOR1* or the *E. coli* pyridoxine biosynthesis genes *pdxA*/*pdxJ*. The *SOR1* group includes fungi, plants, archaebacteria and some eubacteria, whereas the *pdxA*/*pdxJ* group comprises only eubacteria.

Here we describe the crystal structure of *E. coli* PNP synthase (PdxJ) that catalyzes the final step in bacterial vitamin B_6 biosynthesis. Furthermore, the crystal structure of an enzyme-product complex that defines the precise active site environment and reveals conformational changes that accompany binding of products is presented.

OVERALL STRUCTURE

The X-ray structure of native PNP synthase was solved by the single isomorphous replacement method (SIRAS) and refined at 2.0 Å resolution to an R factor of 20.6% (Table 1). The oligomeric state of PNP synthase observed in the crystal is the same as in solution [14]. It is an octameric enzyme in which the subunits are organized with 422 (D4) point group symmetry (Figure 2a). In the $C222_1$ crystal form, the fourfold rotation axis coincides with the crystallographic a axis corresponding to four monomers per asymmetric unit (named A, B, C, and D) that are related by noncrystallographic (NCS) 222 symmetry. The octamer has overall dimensions of 97 x 97 x 77 $Å^3$ and looks like a thick-walled cylinder that is penetrated by a solvent-filled channel of approximately 12 Å

diameter. In this cylinder, the constituting subunits are oriented such that their active sites point away from the internal channel and face the solvent region.

	Native	**EP**
Data collection		
Resolution (Å)	25.0 – 2.0	25.0 – 2.3
Cell parameter unit cell (Å)	a=131.1	A=128.8
	b=155.3	b=156.3
	c=129.8	c=127.5
Reflections		
Observed / unique	345,047 / 87,995	110,743 / 54,860
I / σ (I)		
overall / outer shell	8.6 / 2.1	9.2 / 3.6
R_{merge}[a]		
overall / outer shell	5.6 / 45.2	4.6 / 20.8
Completeness		
overall / outer shell	98.7 / 98.5	96.2 / 95.7
Refinement		
Number of atoms in refinement	7,937	8,144
protein / solvent / ligand	7,190 / 747 / 0	7,330 / 734 / 80
Average B (Å^2)	39.7	36.4
protein / solvent / ligand	39.4 / 42.1 / -	36.0 / 39.1 / 43.2
r.m.s. deviation		
bonds / angles / bonded B's	0.011 / 1.53 / 3.09	0.011 / 1.54 / 2.33
R_{factor}[b] / R_{free}[c]	20.6 / 25.3	18.7 / 24.5

[a] $R_{merge}=\sum_{hkl}| I - I|/\sum_{hkl}|I|$

[b] $R_{factor}=\sum_{hkl}||F_{obs}| - |F_{calc}||/\sum_{hkl}|F_{obs}|$

[c] R_{free} is the R-value calculated with 5% of the data that were not used for the refinement.

Table 1. Data Collection and Refinement Statistics.

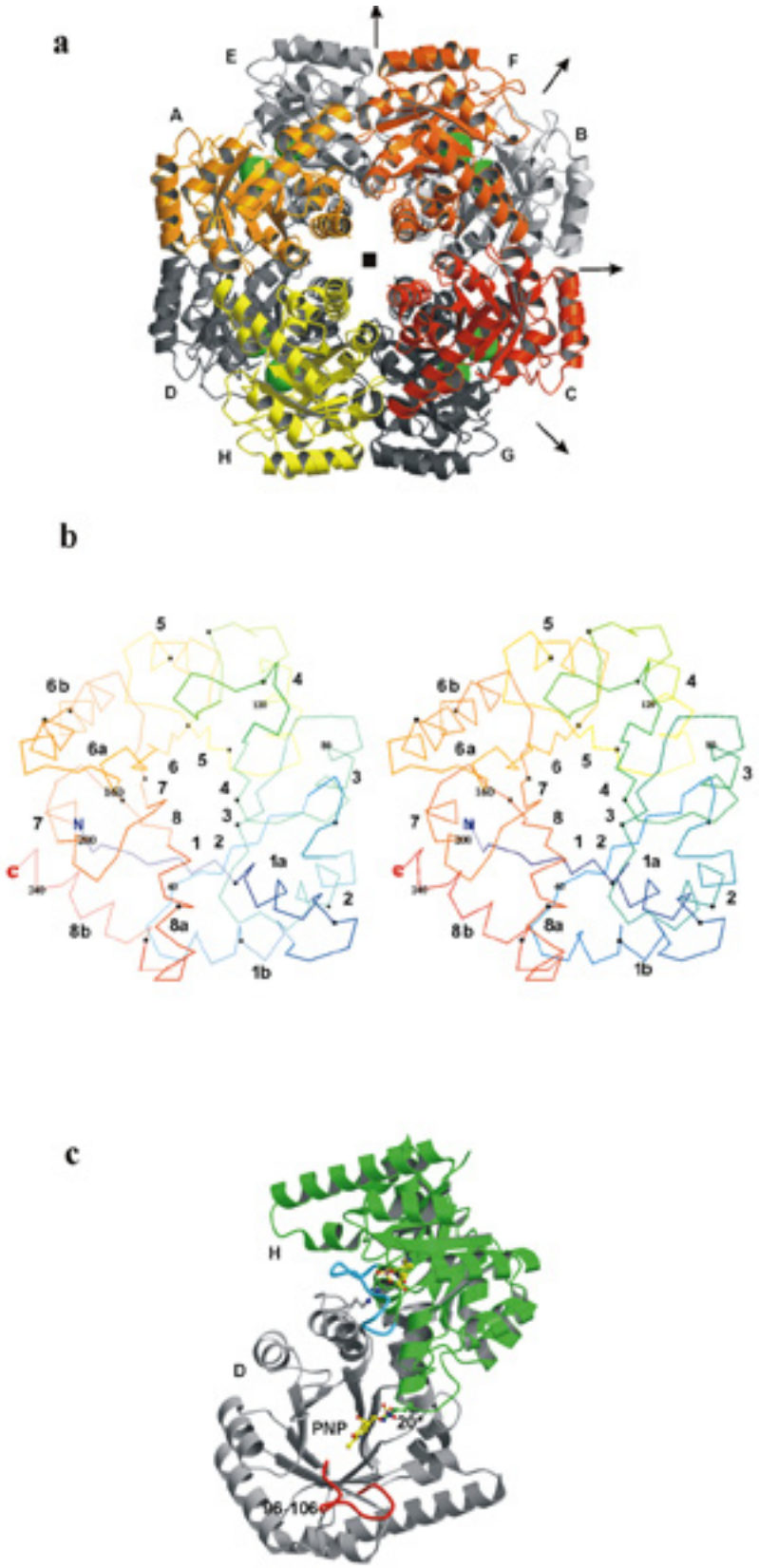
a
E
F
A
B
D
C
H
G
b
5
6b
4
6a
6
5
3
7
4
7
N
8
3
1
2
c
1a
2
8a
8b
1b
c
H
D
PNP
96-106

Figure 2 Overall Structure of PNP Synthase. (a) Quaternary assembly. The octamer can be regarded as a tetramer of active dimers with indicated 422 symmetry. The nomenclature of the monomers as well as the location of the active sites (green balls) are given. The monomers of the upper tetramer ring are colored from red to yellow, the lower ones from light to dark grey. (b) Stereoview C^{α} trace of the PNP synthase TIM barrel. The protein chain was marked every ten residues and numbered every forty. The nomenclature of α-helices and β-strands is given. (c) Active dimer. The flexible loop 4 is highlighted in red (monomer D) and in cyan (monomer H). Arg20 that protrudes into the adjacent active site and the bound product molecules PNP and P_i are shown in a ball-and-stick model. These illustrations and Figure 5 were produced with MOLSCRIPT [30] and RASTER3D [31], Figures 3a and 4 with SETOR [32] and Figures 3b and 6 with DINO [33].

The monomer of *E. coli* PNP synthase is comprised of one compact domain showing the frequently observed $(\beta/\alpha)_8$ or TIM barrel fold (for a review see [15]), where the eight-membered cylindrical β sheet is surrounded by eight helices as illustrated in Figure 2b. Interestingly, a hydrophilic channel is observed in the center of the TIM barrel. The water molecules that are bound in this channel are arranged in a continuous tube that penetrates the protein in full length. The wall of the solvent channel is constructed by four rings of polar residues that project from alternating β strands. From the N- to the C-terminal end of the barrel, these layers are composed of residues Arg68-His210-Phe151-Phe90, Ser131-Asn70-Glu211-Asn190, Glu153-Cys92-Thr43-Asn213 and Glu72-Asn9-His193-Phe133. Similarly to other $(\beta/\alpha)_8$ structures, all of the α helix/β strand turns at the N-terminal end of the barrel are comprised of only three or four residues, while the loops at the C-terminal end, between β strands and subsequent helices, are much longer and build up the active site. The numbering of these loops refer to the preceding β strands, *e.g.,* loop 6 follows strand 6. The C-terminal loops range in length from 3 to 19 residues and harbor additional secondary structural elements, namely helices 1a, 6a and 8a. In the β barrel of PNP synthase, these extra helices are located at the side from which contacts to

neighboring monomers originate. Consistently, helices 1a, 6a and 8a mainly build up the three distinct intersubunit interfaces. One of the loops at the C-terminal end of the β-barrel (loop 4) could not be fully interpreted in the electron-density of monomers A, B and C and exhibited high disorder factors in monomer D (average B value = 63.8 $Å^2$). However, the backbone and most of the side chain atoms of loop 4 show continuos and unambiguous electron density in monomer D.

The PNP synthase octamer is organized as a tetramer of dimers AE, BF, CG and DH. The $(\beta/\alpha)_8$ domains of the corresponding monomers interact extensively about an intervening crystallographic two-fold axis, such that their barrel axes are approximately perpendicular to each other (Figure 2c). The dimer axis passes between the cores of helices 1a and the C-terminal ends of helices 8b that come close together at the dimer interface and form two nearly perpendicularly arranged α helix bundles 1a/8b* and 1a*/8b. Most notably, helix 1a is directed by various specific interactions towards the active site of the neighboring subunit. Arg20, which is part of the C-terminal loop of helix 1a, is even protruding into the adjacent active site, where it fulfills important mechanistic functions. Thus, the "shared" active site strongly suggests that the dimer is the active unit of PNP synthase. Its formation shields 1120 $Å^2$ per monomer, i.e., 10.6 % of the entire monomer surface, while the other monomer-monomer contacts are considerably smaller. The contact areas between the monomers AD, AF and AH comprise 5.0%, 2.8% and 2.7% of the accessible monomer surface, respectively. All dimers within the octamer interact in an identical manner. The corresponding contacts are mediated by the helix-loop-helix motifs of helices 1a-1b, 6a-6b, and 8a-8b and comprise mainly polar interactions. While the 6a-6b motif including residues 161 to 169 is capping

the N-terminal end of the β barrel of the neighboring subunit (interactions AF and AH in the upper tetramer ring of the octamer in Figure 2a), the other two segments establish the symmetric side-by-side dimer-dimer contacts between A and D.

THE ENZYME-PRODUCT COMPLEX

The loops at the solvent-accessible, C-terminal end of the β barrel form a deep cavity that provides the enzyme's active site. The pronounced size of this pocket (11 Å x 14 Å wide, 9 Å deep) should easily accommodate the proposed PNP synthase substrates DXP and AAP, the intermediates of the reaction and the product PNP. To identify individual active site residues, the PNP synthase crystals were soaked with the products of the reaction, PNP and P_i. The original (F_o-F_c) density maps indicated unequivocally the location of the product molecules, which were tightly bound in the C-terminal groove of each TIM barrel subunit, as shown in Figure 3. Selected interatomic distances between protein and ligands are given in Table 2.

a

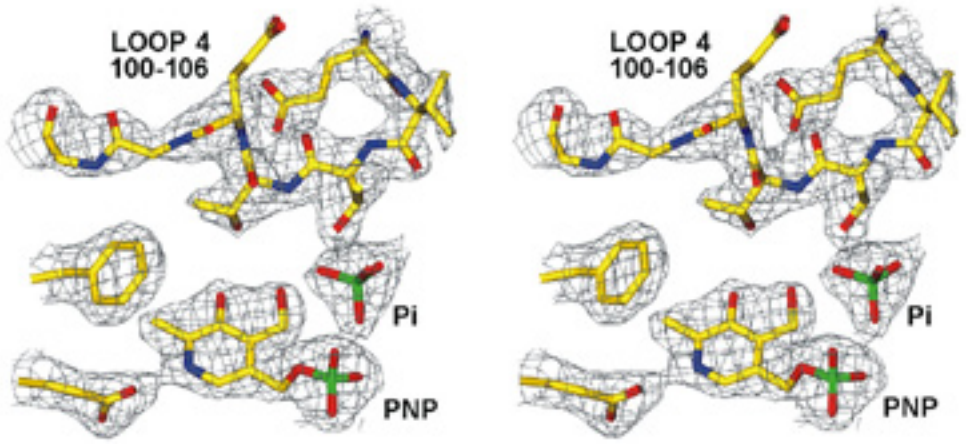

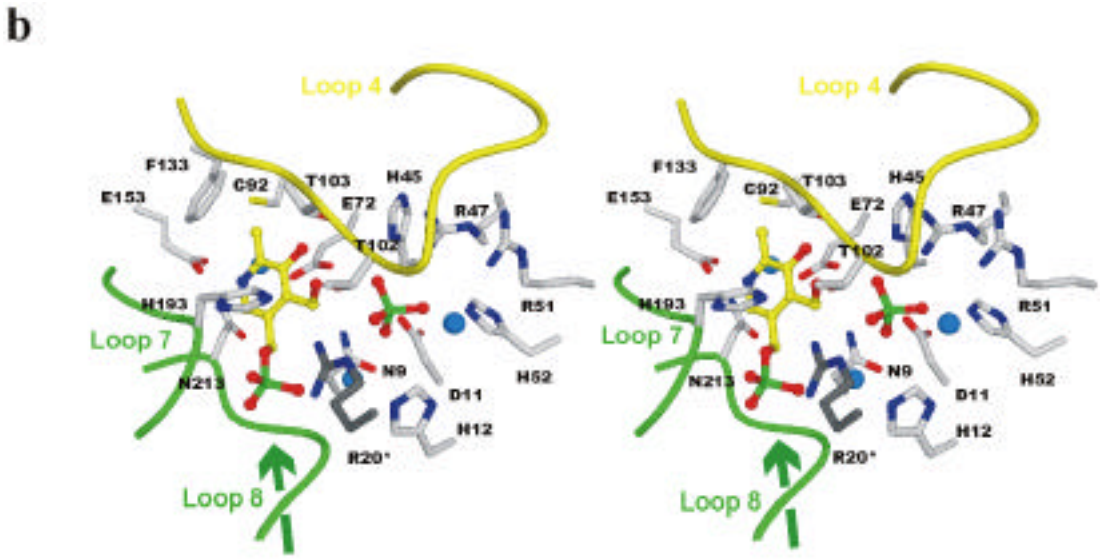

Figure 3. Active Site of PNP Synthase in its Closed Form. (a) Stereoview of the electron density of the bound ligands. The $2F_o–F_c$ simulated annealing omit map (resolution 2.3 Å, contour level 1.1σ) was calculated by omitting the bound ligands and loop 4 residues 96-106 from phase calculation. The portion of the model shown comprises PNP and P_i , part of the flexible loop 4 that protrudes into the active site and the two active site residues Phe133 and Glu153. (b) Detailed active site architecture of the closed EP form. For clarity, the carbon atoms of the ligands and the C^{α}-trace of loop 4 are shown in yellow, water molecules as blue balls and the backbone of the P1-binding site constructed by loops 7 and 8 in green. The macrodipole of helix 8a is indicated.

Formation of the ternary complex led to structural adjustments in the active site, particularly by rearrangement of loop 4 and by reorientation of residues directly contacting the bound ligands. Three different states of the PNP synthase could be reproducibly observed within the crystallographic asymmetric unit of the enzyme-product (EP) complex. While monomer A was always present in a “closed” conformation (Figure 3b), in which loop 4 shields the active site from solvent, monomer D adopted the “open” form. For monomers B and C, the electron density of loop 4 residues 96–106 was not interpretable. Obviously, the different active site environments observed in monomers A, B/C, and D represent three possible states that PNP synthase may adopt during the catalytic cycle. However, the reason for the nonequivalence of the PNP synthase

monomers remains unclear, since all monomers display similar crystal contacts and overall folds (235 C^{α} atoms were aligned with an average rmsd of 0.34 Å). One remarkable difference is the binding of a phosphate ion in the active site of monomer A. The average B factor of the P_i (54.1 $Å^2$) is slightly higher than the B factors of the surrounding residues (45.6 $Å^2$) and the PNP (33.5 $Å^2$). Attempts to refine a P_i at an equivalent position in monomer B, C and D failed as judged from B factors > 150 $Å^2$ and negative difference electron densities. In the superposition performed with the program O [16], 242 C^{α} atoms of the free enzyme were aligned with the open complexed state (r.m.s. deviation of 0.34 Å) and 235 C^{α} atoms with the closed conformation (rmsd of 0.39 Å).

In both open and closed states, the PNP molecule is anchored predominantly through its phosphate group. The corresponding phosphate-binding site, which we refer to as P1 site, is located between loop 7 and loop 8 and is similarly constructed as those of other TIM barrel proteins (see below). Five hydrogen bonds between protein and PNP are discernible, including the main chain amide nitrogens of Gly194, Gly215, His216, and the guanidino group of Arg20*. The two hydrogen bonds with Arg20* are strengthened by charge-charge interactions. Binding of the PNP phosphate is further improved by interaction with the macrodipole of helix 8a, a feature frequently seen in phosphate-binding proteins [17]. The PNP pyridine system is sandwiched between His193 and Glu72. His193 is positioned at the solvent exposed side and is hydrogen bonded to the hydroxylic group of Thr102 and to NE2 of His155. By these interactions, the ring plane of His193 is oriented almost perpendicular to the plane of the PNP pyridine ring. On the opposite side of PNP, at the side directed towards the protein interior, the carboxylate group of Glu72 is facing the pyridine ring atoms. The interatomic distances between

Glu72-OE1/2 and PNP-N1, C2, C3, C4, C5, and C6 are 3.4, 3.2, 3.3, 4.0, 4.3 and 4.0 Å, respectively. The PNP is further bound by the carboxylate group of Glu153, which forms a strong hydrogen bond/salt bridge with the pyridine N1. The side chain of this glutamate is fixed in proper orientation by the main chain NH of Gly192, the sulfhydryl group of Cys92, the amide nitrogen of Asn213, and a well-defined water molecule that is bridging Glu72 and Glu153 carboxylate groups. The PNP methyl group at C2 points to the aromatic side chain of Phe133 and undergoes van der Waals interactions with each of the ring atoms. The hydroxyl group at C3 interacts with the hydroxylic group of Thr103, one of the loop 4 residues, and with the carboxylate OE2 of Glu72. As stated before, a P_i was identified in the closed state of the EP complex at a second phosphate binding site, the P2 site. Contrary to the P1 site, this site is constructed by side chains of dominantly basic residues. Strong hydrogen bonds are formed between P_i and Arg20*, Asp11, His12, Arg47, His52, Thr102, and Thr103. Arg20* and Arg47, especially, should be involved in charge compensation of the P_i, as deduced from their close distance. Finally, two well-defined water molecules are observed in close distance to both phosphate groups: one water molecule is wedged between them and the second is bound to P_i at the P2 site.

In the open conformation, characteristic structural differences in the active site are the consequence of the expulsion of loop 4 and the release of P_i. Most strikingly, solvent has now direct access to the PNP C3 and C4 positions and to the P2 site. Due to the absence of its interaction partner, Thr102, the hydroxyl group at PNP-C4' reorientates and binds strongly to Asn9. Similarly, the interactions of His193 with Thr102 and Arg47 with Glu100 are disrupted upon active site opening. As a consequence, Arg47, one of the most prominent P_i binding residues, adopts a different conformation and moves away from the

active site. The remaining interactions between PNP synthase and PNP are conserved in the open form, some with slightly different interatomic distances (Table 2).

PNP synthase	**Ligands**	**Distance (Å)**	
		EP open	**EP closed**
Asn9-ND2	PNP-O4'	3.0	5.0
Asp11-OD2	PNP-O4'	3.2	5.4
	P_i-OP3	-	2.7
His12-ND1	P_i-OP2	-	4.6
-NE2	PNP-OP2	4.6	4.7
	P_i-OP1	-	4.0
His45-ND1	PNP-O3'	4.8	4.4
	PNP-O4'	6.5	4.5
	Pi-OP4	-	3.1
Arg47-NH1	P_i-OP2	-	2.7
His52-NE2	P_i-OP2	-	2.9
Glu72-OE1	PNP-N1	3.5	3.4
	PNP-O3'	3.4	3.8
-OE2	PNP-O3'	2.7	2.9
Thr102-OG1	P_i-OP1	-	2.8
Thr103-OG1	PNP-O3'	-	2.8
	PNP-O4'	-	3.0
	P_i-OP4	-	3.9
Glu153-OE1	PNP-N1	2.5	2.7
His193-ND1	PNP-O4'	3.5	4.4
	PNP-OP1	4.5	4.0
Gly194-N	PNP-OP1	2.7	2.7
Gly215-N	PNP-OP3	2.6	2.7
His216-N	PNP-OP2	2.7	2.7
Arg20*-NH1	PNP-OP1	2.5	3.4
	PNP-OP2	2.8	3.1
-NH2	PNP-O4'	4.3	3.7
	PNP-OP2	2.9	3.3
	P_i-OP1	-	3.5

[a] The table summarizes those residues that enclose the ligands. To indicate differences between the discussed structures, sometimes also distances > 4.0 Å are included.

Table 2 Interatomic Distances Between PNP Synthase and Bound Ligands[a].

The largest differences during the open-closed transition are observed for loop 4, which is folded away from the active site in the unliganded form but reorientates upon interaction with proper ligands and closes the active site like a lid. The resultant shielding should help to avoid unwanted side reactions and to stabilize chemically labile intermediates. The present crystal structure of the product-complexed PNP synthase provides a simultaneous view on these two distinct states (Figure 4). Thereafter, occupation of both phosphate binding sites P1 and P2 is the minimum prerequisite to induce rearrangement of loop 4.

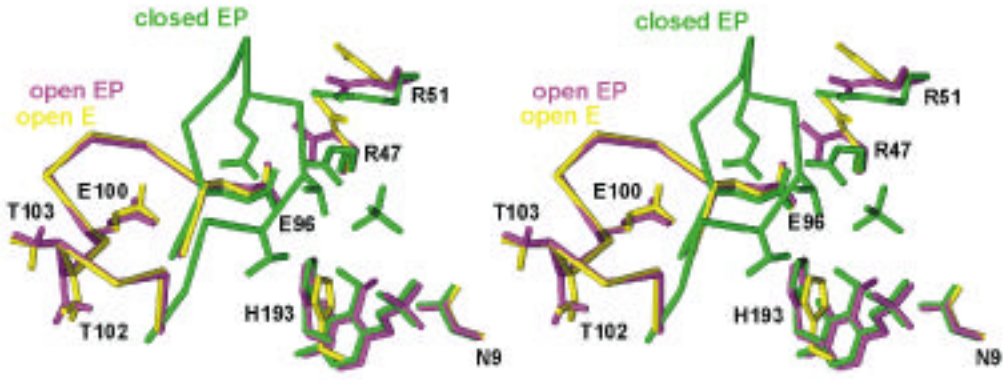

Figure 4. Open-Closed Transition of PNP Synthase. Stereoview of residues involved in the conversion from open (yellow, free enzyme; magenta, open EP form) to closed (green, closed EP form) conformation. The C^{α}-trace of loop 4 is indicated as well as the bound ligands.

The mechanism of active-site closure should be based mainly on the thermodynamic equilibrium between the open and closed states. In the open state, loop 4 is solely held in place by a few van der Waals contacts and by two hydrogen bonds formed between Glu104-Arg174 and Glu100(O)-Asp108(NH). The remaining loop residues are not involved in any specific interactions, explaining the inherent mobility of loop 4, which is an essential requirement for facile open-closed interconversion. Most likely, the flexible loop 4 of the free enzyme fluctuates between both states until proper ligands are bound.

In the presence of products, the open-closed equilibrium is shifted towards the closed form, which is stabilized by numerous interactions over the open form. The transition may be triggered by binding a phosphate group at the P2 site, leading to reorientation of the side chains of Arg47 and Arg51. The guanidino group of Arg47 moves 3.5 Å toward the active site and fixes the side chain of the flexible Glu100 that, in turn, can strongly interact with the amide nitrogen of "hinge" residue Glu96, stabilizing its closed conformation. The backbone of residues 96–103 flips inward, and, successively hydrogen bonds are formed between Arg98(O)-Arg51, Glu100(O)-Arg51, Val101(O)-Arg51, Thr102-P_i, Thr102-His193, and Thr103-PNP(4'OH). At the opposite end of loop 4, the two glycine residues Gly105 and Gly106 allow sufficient backbone flexibility to complete the transition. Destabilization of the closed state may be due to disruption of the hydrogen bonds between Thr103-PNP and Thr102-His193, as seen in the open EP complex. Here, the 4'OH group of PNP is rotated away from loop 4 and interacts with the side-chain of Asn9. Thus, the concerted breaking of hydrogen bonds with residues 102-104 seems to initiate active site opening and concurrent release of P_i.

MECHANISTIC IMPLICATIONS

Several mechanistic proposals have been put forward how PNP synthase catalyzes the final step in vitamin B_6 biosynthesis [7-9]. The complex multistep mechanism involves Schiff-base formation, water elimination and addition, P_i elimination, ring closure, and various proton shifts, as shown in Figure 1. The biochemical characterization of this mechanism is hampered by the fact that the AAP substrate is highly unstable. In most

cases, the enzymatic analysis has to be coupled to the PdxA catalyzed reaction, complicating the derivation of individual kinetic parameters. While the precise sequence of individual steps remains a matter of speculation, several important mechanistic features can be deduced from the structural work. Since all of the mechanistically important residues are invariant in the PNP synthase family (data not shown), a common mechanism can be anticipated.

PNP synthase operates as a two-state enzyme. The open state accepts substrates and releases products, while the chemistry occurs in the closed state, where the active site is shielded from solvent. Substrates and inhibitors can bind principally through three kinds of interactions: with the P1 site, with the P2 site, and with the "specificity" pocket. The latter is located in the center of the β barrel and defined by residues that line the pyridine moiety in the EP complex, including Asn9, His45, Glu72, Thr102, Thr103, Phe133, Glu153, and His193. The transition to the closed state, where loop 4 (Glu96-Gly106) shields the active site, depends on a multitude of specific interactions between enzyme and ligands. The key residues involved in this transition are Arg47, Arg51, and the loop 4 residues Glu96, Glu100, Thr102, and Thr103. Since residues of mobile loop 4 are not directly involved in catalysis, the main purpose of active site closure seems to be the exclusion of water molecules to avoid unspecific side reactions and, in terms of the transition state theory, stabilization of occurring reaction intermediates by donating several hydrogen bonds. One interesting feature of the PNP synthase structure is the solvent channel that runs through the β barrel. This tunnel explains how water molecules can be liberated from the closed active site. The water tubes in all monomers of the E and

EP form are not fully filled, suggesting a water-relay system that should buffer water molecules, which are released during the catalyzed reaction (Figure 5a).

Specific roles of catalytic groups may be inferred from their relative orientations to the bound product molecules PNP and P_i (Figure 5b). Thereafter, Glu72 appears to be the central acid-base catalyst of PNP synthase. It is located such that it can approach each of the pyridine ring atoms of occurring reaction intermediates. Moreover, this glutamate interacts directly with the hydroxylic function at PNP-C3. In addition to its outstanding spatial position, Glu72 is part of a pronounced proton/charge-relay system including His45, Glu153, and a well-defined water molecule that was present in all analyzed active-site cavities. This system seems to achieve the mutual coupling between the electronic configuration of reaction intermediates and the Glu72 protonation state. The crystal structures indicate that binding of a phosphate ion at the P2 site causes reorientation of the presumably protonated His45 side-chain and concomitant disruption of the His45-Glu72 interaction, thereby increasing the basicity of Glu72. The pK_a of Glu72 is further influenced by the water-mediated interaction with Glu153. The latter glutamate is optimally positioned to stabilize a developing positive charge on the Schiff-base nitrogen. A similar interaction is observed frequently for PLP-dependent enzymes, where an aspartate neutralizes the positively charged pyridine N1 and increases the electron-sink character of the cofactor [18]. His193 is the only proton donor/acceptor on the other side of the pyridine ring, facing the solvent region.

The structure of the EP complex suggests that a phosphate, which is covalently bound to the Schiff-base conjugate, cannot occupy the P2 pocket. Thus, the enzyme appears to facilitate cleavage of the scissile DXP-phosphate, the main driving force of the reaction,

by providing a large anion hole constructed by several basic residues that is only available for a released phosphate group.

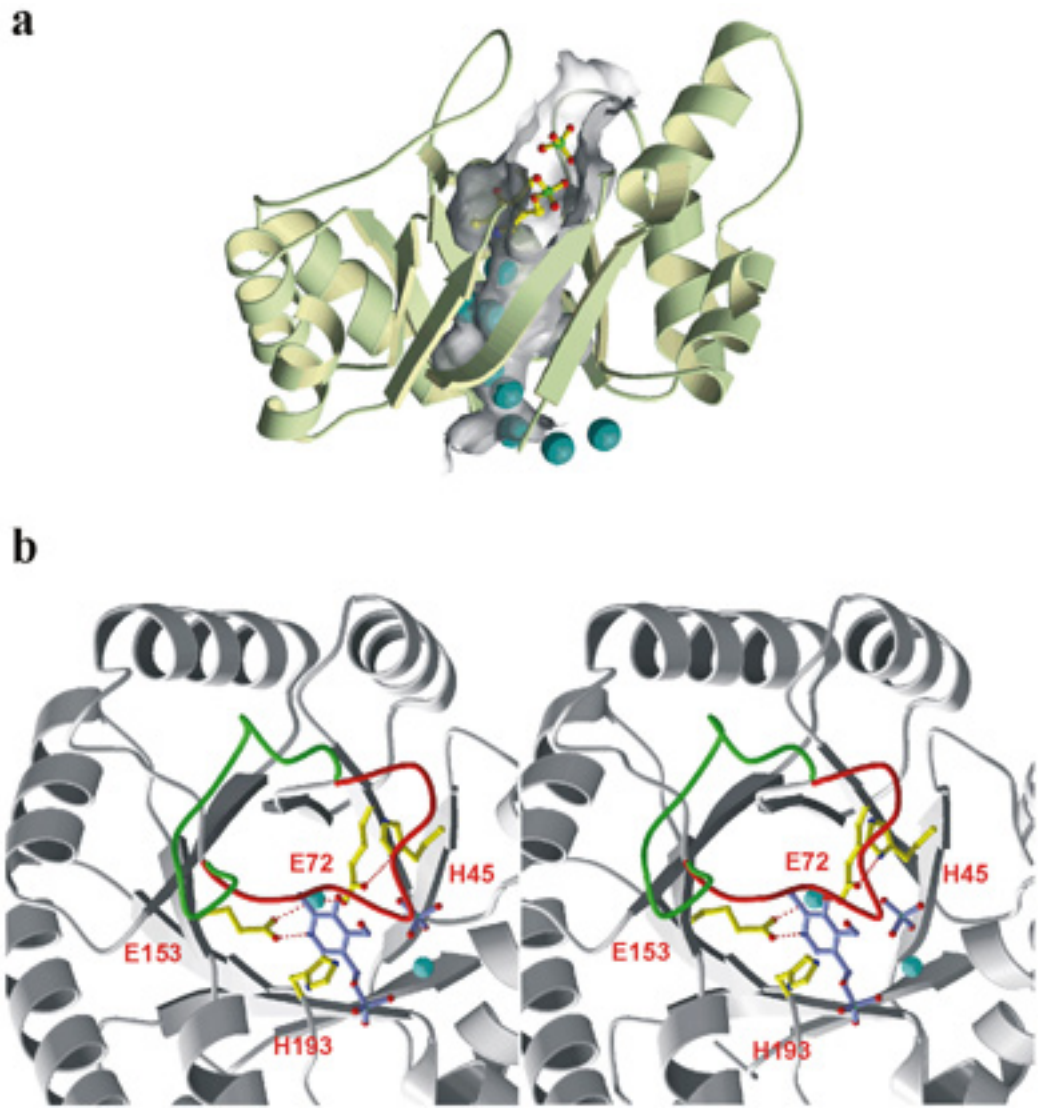

Figure 5. Mechanistic Features of PNP synthase. (a) Solvent channel in the center of the PNP synthase barrel. The illustrated accessible surface was calculated by omitting all water molecules. The bound products and the pore waters are given in ball-and-stick mode. (b) Catalytically important residues. PNP and P_i are hold in lila, water molecules are shown as cyan balls. In the EP complex, both open (green) and closed (red) states were observed visualizing how the reaction products can be released from the active site of PNP synthase. His45, Glu72, Glu153 and an active site water set up one charge/proton relay system on the protein facing side of the ligands, His193 is situated as potential acid-base catalyst on the opposite, solvent-directed site.

COMPARISON WITH OTHER α/β-BARREL STRUCTURES

Since no related structure of PNP synthase is available up to now, the DALI algorithm was employed for the search of structural homologues. The three TIM barrel enzymes of tryptophan synthesis, i.e., indoleglycerolphosphate synthase (IGPS), phosphoribosyl-anthranilate isomerase and the α-subunit of tryptophan synthase, were identified as the most similar structures in the database, with z-scores of 18.6, 18.1, and 16.3, respectively, corresponding to 200 ± 5 C^{α}s, aligned with a rmsd of 2.8 ± 0.2 Å. Furthermore, the multiple structural alignment indicated that none of the deposited $(\beta/\alpha)_8$ barrel folds have structural equivalents to PNP synthase helix 1a, region 155-165, and loop 4. The former two regions determine the oligomeric assembly of PNP synthase, with helix1a being the central element in dimer formation and region 155-160 capping the N-terminus of the β barrel of the adjacent subunit. Loop 4 is crucial for active site closure and carries mechanistically important residues.

The DALI superposition with the most similar structure (i.e., IGPS) is shown in Figure 6a and illustrates that the basic $(\beta/\alpha)_8$ architecture is highly conserved. Only helices 1b, 3, 4 and 7 exhibit deviations in orientation and length. Greater variability is found at the C-terminal loops of the β barrel as the consequence of different catalytic functions. One remarkable difference concerns the origin of the loop that has been proposed to undergo conformational rearrangement upon substrate binding [19]. While IGPS and its related structures have an extraordinary long and highly flexible loop following β strand 6, the corresponding loop of PNP synthase, 15 residues in length, follows strand 4. The most striking similarity in the alignment is a common phosphate binding site. In the three cited

enzymes and in PNP synthase, a phosphate group is bound at equivalent position in the tertiary structure: this group is hydrogen-bonded to the main-chain nitrogens of the N-terminal end of helix 8a and its preceding loop and to the first residues of the loop 7. The charge of the phosphate is compensated partially by the macrodipole of helix 8a that is 6 residues longer in PNP synthase than in IGPS and related structures. The comparison indicates that local sequence similarities are present in the phosphate binding segments. For example, a structurally conserved glycine, Gly194 in PNP synthase, is observed at the N-terminus of loop 7 that is generally followed by a small hydrophobic residue (leucine, isoleucine, valine) and by a small polar residue (serine, threonine, asparagine). Another invariant glycine, Gly215, mediates the connection between β strand 8 and α helix 8a. As proposed earlier [19], a glycine residue in this position set up the phosphate binding site by fixing the relative orientation of strand 8 and helix 8a to each other.

The structure of PNP synthase was also compared with that of alanine racemase, a PLP-dependent enzyme showing the abundant $(\beta/\alpha)_8$ fold (Figure 6b). The z score of the DALI superposition (11.3) is significantly lower than those of the tryptophan biosynthetic enzymes. Remarkably, the position and relative orientation of the PLP cofactor of alanine racemase strongly resembles that of the bound PNP of PNP synthase. In particular, the phosphate binding site appears to be highly conserved. However, PLP and PNP have to serve different purposes in alanine racemase and PNP synthase. While PLP functions as cofactor in alanine racemase, PNP is simply the product of the PNP synthase-catalyzed reaction. This difference is expressed in the crystal structures by the binding modes of the two vitamin B_6 derivatives. In alanine racemase, numerous interactions are undergone with the PLP that precisely adjusts the electronic distribution of the pyridoxal system to

its catalytic demand. In PNP synthase, the key determinants of cofactor reactivity, i.e., Schiff-base formation with an active site lysine and ring stacking interactions with the pyridine system, are absent.

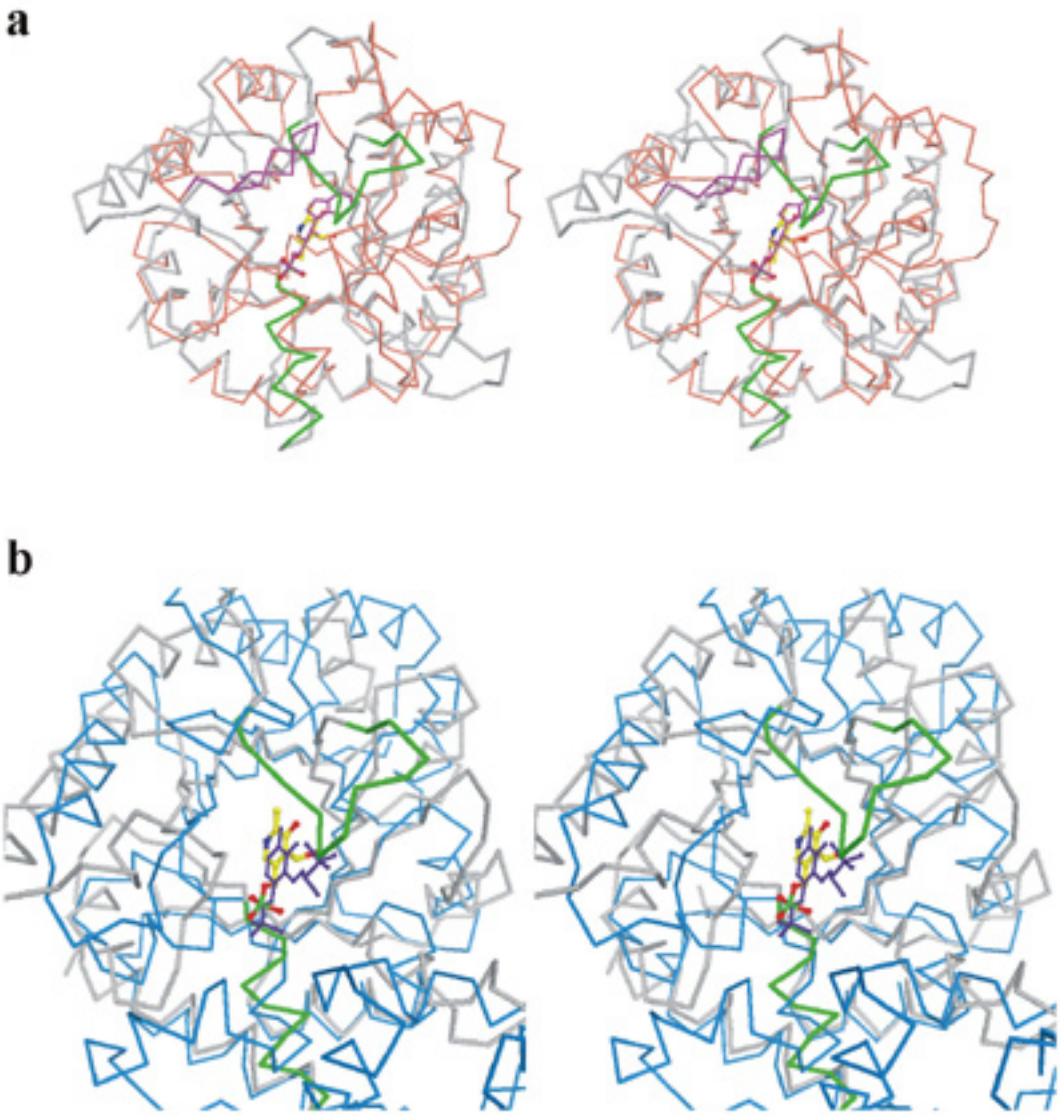

Figure 6. Structural Comparison. DALI superpositions of the open state of PNP synthase (grey) with related TIM-barrel structures. The phosphate-binding helix 8a and the flexible loop 4 are coloured green, the bound PNP by atom-type. (a) Alignment with indoleglycerol 3-phosphate synthase (IGPS, orange). The mobile loop of IGPS and the bound IGP are shown in magenta. (b) Alignment with alanine racemase (blue), showing its PLP cofactor in purple.

In summary, the DALI superpositions reveal a higher degree of similarity between PNP synthase and TIM barrel enzymes that utilize phosphate containing ligands. Additionally, the structural alignments further affirm the common phosphate binding site that is present in a large number of functionally unrelated TIM barrel enzymes [20]. According to the hypothesis of Jensen [21] that divergent evolution proceeded from primitive enzymes with broad substrate specificity, a common primordial phosphate-binding ancestor seems feasible for a large class of $(\beta/\alpha)_8$ barrel proteins.

BIOLOGICAL IMPLICATIONS

Vitamin B_6 (pyridoxol) is an essential component of the human diet since, unlike plants and microorganisms, humans can not synthesize this vitamin. The biologically active forms of vitamin B_6, pyridoxal 5'-phosphate (PLP) and pyridoxamine 5'-phosphate (PMP), act as essential coenzymes in most metabolic conversions of amino acids and in the biosynthesis of antibiotic compounds and deoxysugars. In all organisms, PMP is generated from PLP by transamination, while the latter is derived from pyridoxine 5'-phosphate (PNP) by an O_2-dependent oxidation. Pyridoxine itself can be converted to PNP by an ATP-dependent kinase, which can also mediate the formation of PLP and PMP from the corresponding free alcohols. However, PNP is the only B_6 vitamer that is synthesized *de novo*.

This paper describes the crystal structure of the key enzyme of vitamin B_6 biosynthesis, PNP synthase (PdxJ), which is also the first structurally characterized enzyme in this pathway. In *E. coli*, PNP synthase catalyzes the final step in PNP

biosynthesis, the condensation of 1-amino-acetone 3-phosphate and 1-deoxy-D-xylulose 5-phosphate to yield PNP, inorganic phosphate and two molecules of water. PNP synthase is an homooctamer with 242 amino acid residues per subunit. In the crystal structure of the enzyme, which was determined at 2.0 Å resolution, the subunits fold into a compact TIM barrel domain. Intersubunit contacts are mediated by three "extra" helices, thereby generating a tetramer of symmetric dimers with shared active sites. Structural analysis of PNP synthase complexed with reaction products allowed the identification of the active site, of amino acids critical for catalysis and revealed that during catalysis the active site of the enzyme undergoes a transition from an open to a closed conformation. The open state is supposed to accept substrates and to release products, while most of the catalytic events are likely to occur in the closed state. A hydrophilic channel running through the center of the TIM barrel was identified as the essential structural feature that enables PNP synthase to release the water molecules produced during the reaction from the closed, solvent-shielded active site.

The determination of the structures of the native and product-bound PNP synthase is a first, but indispensable, step towards understanding the complex chemistry by which nature synthesizes one of its most versatile cofactors. Further structural studies to elucidate the precise mode of action in combination with the design of active site mutants to testify mechanistic hypotheses may finally guide the structure-based design of PNP synthase inhibitors. Such inhibitors may become new antibacterial agents and might, thereby, help to overcome the increasing problem of antibiotic resistance. In this context, it should be emphasized that PNP synthase is restricted to a limited number of bacteria, including well-known pathogens like *Neisseria gonorrhoeae*, *Neisseria meningitidis*,

Salmonella typhimurium, *Vibrio cholerae*, and *Yersinia pestis*, which will be advantageous in the development of highly specific drugs.

Acknowledgements

We thank Sandra Scharf for her expert support during protein purification, Constanze Breithaupt for helpful discussions and Gleb P. Bourenkov for assistance during collection of the high resolution data at the DESY beamline BW6.

Accession numbers

The coordinates of the crystal structures of native PNP-synthase and the product-complexed form have been deposited at the Protein Data Bank database and are available under accession codes 1ho1 and 1ho4, respectively.

EXPERIMENTAL PROCEDURES

Crystallization and Data Collection

The PNP synthase enzyme was purified and crystallized as previously reported [8, 14]. Briefly, the best diffracting crystals grew in space group $C222_1$, with lattice parameters a=132.5 Å, b=155.1 Å, and c=130.1 Å containing four monomers per asymmetric unit. High-resolution data of native PNP synthase crystals were collected at the DESY BW6 beamline (Deutsches Elektronen Synchroton, Hamburg, Germany), and yielded a complete 2.0 Å data set. Diffraction data up to 2.3 Å for the EP complex were collected at our in-house Mar Research (Hamburg, Germany) image plate system mounted on a

Rigaku (Tokyo, Japan) rotating anode generator operated at 50kV/100mA with Cu K_α radiation (λ = 1.5418 Å). Best results were obtained by incubating PNP synthase crystals for 1 h in 5 mM PNP/5 mM P_i. Processing of the diffraction data and scaling of the individual structure factors sets were performed with programs of the hkl [22] and the CCP4 package [23], respectively.

Structure Determination and Refinement

The structure solution of PNP synthase succeeded by the SIRAS method with a highly isomorphic thiomersal derivative, for which 12 Hg sites could be identified [14]. The solvent-flattened density map was of sufficient quality for chain tracing and to build the molecular mask with MAMA [24]. Using NCS operators extracted from the heavy atom sites with FINDNCS [25], a 4-fold averaged map, in which the complete model of PNP synthase was built in, was calculated with AVE [24, 26],. Model building was done with the program O [16] implemented on an Indigo2 workstation (Silicon Graphics). For energy-restrained structure refinement, the maximum likelihood algorithms of CNS [27] and the protein parameter set of Engh and Huber (1991) [28] were used. Bulk solvent, overall anisotropic B factor corrections, and NCS restraints (except for residues 96-106) were introduced depending on the behavior of the free R factor index. In later stages, solvent molecules were introduced at stereochemically reasonable positions with high difference electron densities. During the whole refinement the R factor decreased from 35.9 to 20.6% (R_{free} from 37.3 to 25.3%) for all data between 25.0 and 2.0 Å resolution. The final model includes 4 monomers and 747 water molecules and exhibits good stereochemistry (Table 1). In the Ramachandran plot, 92.3% of the residues were found

in the most favorable, 7.5% in the favorable, 0.2% in the generously allowed, and no residue in the disallowed region. For monomers A, B, and C, only poor density was observed for residues 96 to 106 which were omitted from the model. A similar procedure was employed for the EP complex. Several rounds of simulated annealing, positional refinement and B factor optimization with CNS alternated with manual refitting with O. Again, residues 96-106, were highly flexible in monomers B and C but, surprisingly they exhibited different folds in monomers A and D. The ligands (one molecule of PNP per monomer, and P_i in monomer A) were only included in the last round of refinement. The secondary structural elements were used as defined by the program DSSP [29].

REFERENCES

1. Spenser, I.D. and Hill, R.E. (1995). The Biosynthesis of Pyridoxine. Nat. Prod. Rep. *12*, 555-565.
2. Hill, R.E. and Spenser, I.D. (1986). Biosynthesis of vitamin B6. In *Vitamin B6, Pyridoxal Phosphate, Part A*, D. Dolphin, R. Poulson, and O. Avramovic, eds. (New York: Wiley Interscience), pp. 417-476.
3. Tryfiates, G.P. (1986). Pyridoxal phosphate and metabolism. In *Vitamin B6, Pyridoxal Phosphate, Part B*, D. Dolphin, R. Poulson, and O. Avramovic, eds. (New York: Wiley Interscience), pp. 421-448.
4. Dempsey, W.D. (1987). Synthesis of pyridoxal phosphate. in *Escherichia coli and Salmonella typhimurium: Cellular and molecular biology*, F.C. Neidhardt, *et al.*, eds. (Washington, D.C.: American Society for Microbiology), pp. 539-543.
5. Yang, Y., Zhao, G.S., and Winkler, M.E. (1996). Identification of the *pdxK* gene that encodes pyridoxine (vitamin B-6) kinase in *Escherichia coli* K-12. FEMS Microbiol. Lett. *141*, 89-95.
6. Cane, D.E., Hsiung, Y.J., Cornish, J.A., Robinson, J.K., and Spenser, I.D. (1998). Biosynthesis of vitamin B-6: The oxidation of 4- (phosphohydroxy)-L-threonine by PdxA. J. Am. Chem. Soc. *120*, 1936-1937.
7. Cane, D.E., Du, S.C., Robinson, J.K., Hsiung, Y., and Spenser, I.D. (1999). Biosynthesis of vitamin B-6: Enzymatic conversion of 1-deoxy-D- xylulose-5-phosphate to pyridoxol phosphate. J. Am. Chem. Soc. *121*, 7722-7723.
8. Laber, B., Maurer, W., Scharf, S., Stepusin, K., and Schmidt, F.S. (1999). Vitamin B-6 biosynthesis: formation of pyridoxine 5 '-phosphate from 4-(phosphohydroxy)-L-threonine and 1-deoxy-D-xylulose-5- phosphate by PdxA and PdxJ protein. FEBS Lett. *449*, 45-48.

9. Cane, D.E., Du, S.C., and Spenser, I.D. (2000). Biosynthesis of vitamin B-6: origin of the oxygen atoms of pyridoxol phosphate. J. Am. Chem. Soc. *122*, 4213-4214.
10. Ehrenshaft, M., Jenns, A.E., Chung, K.R., and Daub, M.E. (1998). SOR1, a gene required for photosensitizer and singlet oxygen resistance in Cercospora fungi, is higly conserved in divergent organisms. Mol. Cell *1*, 603-609.
11. Bilski, P., Li, M.Y., Daub, M.E., Ehrenshaft, M., and Chignell, C.F. (1999). Antioxidant properties of pyridoxine and its derivatives: quenching of singlet oxygen (1O2). Free Radic. Biol. and Med. 25S, 28.
12. Ehrenshaft, M., Bilski, P., Li, M.S., Chignell, C.F., and Daub, M.E. (1999). A highly conserved sequence is a novel gene involved in de novo vitamin B6 biosynthesis. Proc. Natl. Acad. Sci. *96*, 9374-9378.
13. Osmani, A.H., May, G.S., and Osmani, S.A. (1999). The extremely conserved *pyroA* gene of *Aspergillus nidulans* is required for pyridoxine synthesis and is required indirectly for resistance to photosensitizers. J. Biol. Chem. *274*, 23565-23569.
14. Garrido-Franco, M., Huber, R., Schmidt, F.S., Laber, B., and Clausen, T. (2000). Crystallization and preliminary x-ray crystallographic analysis of PdxJ, the Pyridoxine 5'-phosphate synthesizing enzyme. Acta Cryst. Sect. D *56*, 1045-1048.
15. Reardon, D. and Farber, G.K. (1995). Protein motifs. 4. The structure and evolution of alpha/beta barrel proteins. FASEB J. *9*, 497-503.
16. Jones, T.A. and Kjelgaard (1991). *O-The Manual* (Uppsala: Sweden).
17. Hol, W.G., van Duijnen, P.T., and Berendsen, H.J. (1978). The alpha-helix dipole and the properties of proteins. Nature *273*, 443-446.
18. Jansonius, J.N. (1998). Structure, evolution and action of vitamin B6-dependent enzymes. Curr. Opin. Struct. Biol. *8*, 759-769.
19. Willmanns, M., Schlagenhauf, E., Fol, B., and Jansonius, J.N. (1990). Crystallization and structure solution at 4 Å resolution of the recombinant synthase domain of N-(5'-phosphoribosyl)anthranilate isomerase: indole-3-glycerol-phosphate synthase from *Escherichia coli* complexed to a substrate analogue. Protein Eng. *3*, 173-180.
20. Branden, C.I. (1991). The TIM barrel: the most frequently occurring folding motif in proteins. Curr. Opin. Struct. Biol. *1*, 978-983.
21. Jensen, R.A. (1976). Enzyme recruitment in evolution of new function. Annu. Rev. Microbiol. *30*, 409-425.
22. Otwinowski, Z. and Minor, W. (1997). Processing of X-ray diffraction data collected in oscillation mode. Methods Enzymol. *276*, 307-326.
23. Collaborative Computing Project Number 4 (1994). The CCP4 suite - programs for protein crystallography. Acta Cryst. Sect. D *50*, 760-763.

24. Kleywegt, G.J. and Jones, T.A. (1994). Halloween... Masks and Bones. In *From First Map to Final Model,* S. Bailey, R. Hubbard, and D. Waller, eds. (Warrington, UK: SERC Daresbury Laboratory), pp. 59-66.
25. Lu, G.G. (1999). FINDNCS: a program to detect non-crystallographic symmetries in protein crystals from heavy-atom sites. J. Appl. Crystallogr. *32*, 365-368.
26. Jones, T.A. (1992). A, yaap, asap, @#*? A set of averaging programs. In *Molecular Replacement,* E.J. Dodson, S. Gover, and W. Wolf, eds. (Warrington: SERC Daresbury Laboratory), pp. 91-105.
27. Brünger, A.T. (1992). *XPLOR (Version 3.1) Manual* (New Haven and London: Yale University Press).
28. Engh, R.A. and Huber, R. (1991). Accurate bond and angle parameters for X-ray protein-structure refinement. Acta Cryst. Sect. A *47*, 392-400.
29. Kabsch, W. and Sander, C. (1983). Dictionary of protein secondary structure: pattern recognition of hydrogen bonded and geometrical features. Biopolymers *22*, 2577-2637.
30. Kraulis, P.J. (1991). MOLSCRIPT: a program to produce both detailed and schematic plots of protein structures. J. Appl. Crystallogr. *24*, 946-950.
31. Merrit, E.A. and Murphy, M.E.P. (1994). RASTER3D Version 2.0. A program for photorealistic molecular graphics. Acta Cryst. Sect. D *50*, 869-873.
32. Evans, S.V. (1993). Setor - hardware-lighted 3-dimensional solid model representations of macromolecules. J. Mol. Graph. *11*, 134-141.
33. Philippsen, A. (1999). Visualizing Structural Biology. *http://www.bioz.unibas.ch/~xray/dino*.